IEEE/CSC SUPERCONDUCTIVITY NEWS FORUM (global edition) January 2015.
This ASC 2014 manuscript 2EPo1D-07 published online in *IEEE Trans. Appl. Supercond.* *(IEEE XPLORE)* DOI: 10.1109/TASC.2014.2359764, on September 23, 2014.

Dipole sensitive, homogeneous-field compensated high-T_c dc SQUID

A. Guillaume, F. Ludwig, D. Kajevic, J. M. Scholtyssek, and M. Schilling

***Abstract*—Magnetic nanoparticles (MNP) are of great interest for industrial and medical applications. Therefore, the properties of the particles must be well known. In order to determine parameters such as particle size and particle size distribution, several magnetic measurement schemes have been developed. For the measurement of small amounts of particles, a sensor design with high dipole sensitivity is required while homogenous excitation fields must be shielded or compensated. The spatial dimensions need to be tuned to the sample size in order to maximize the coupling efficiency. In this paper, we present a new sensor design employing a high-T_c $YBa_2Cu_3O_7$ (YBCO) superconducting quantum interference device (SQUID) which is inductively coupled to a surrounding superconducting compensation loop. The design offers a tunable coupling inductance in order to achieve a compensation of the flux coupled into the SQUID by an external magnetic field. We choose a square SQUID design which is positioned in the axis of symmetry of the compensation loop in order to compensate spatial homogenous and first order gradient magnetic fields. The SQUID is operated in a flux locked loop (FLL) with bias reversal. We investigate the dependence of the performance on the compensation loop layout. Design limitations are demonstrated and the SQUID noise is characterized with and without applied magnetic field.**

***Index Terms* — high-T_c SQUID, SQUID noise, dipole sensitivity, magnetic shielding, magnetic nanoparticles**

I. Introduction

MAGNETIC NANOPARTICLES (MNP) – generally consisting of a magnetic core and a shell which protects the core and allows a specific functionalization – can be employed in a variety of applications in medicine and bioanalysis, e.g., as contrast agent for magnetic resonance imaging (MRI) or in immunoassays.

An ensemble of MNPs exhibits a magnetization M given by the sum of the magnetic moments $\boldsymbol{m}$ of the single particles. The resulting magnetic field can be regarded as dipole field consisting of the dipole fields of the single particles. The magnetic moments tend to align in a magnetic field $\boldsymbol{H}$ resulting in a magnetization given by the Langevin function where the argument is formed by the magnetic energy $\boldsymbol{m}\cdot\boldsymbol{H}$, which causes the alignment, in competition with the thermal energy $k_B T$. Magnetic characterization schemes are based on the measurement of the particles' magnetization in or after exposing the particles to static, ac or pulsed magnetic fields. Magnetorelaxometry (MRX) delivers valuable information about the particle size distribution and is well established with fluxgate sensors [1] and with low-T_c [2]-[6] and high-T_c [7]-[14] SQUIDs. The sensors, designed as magnetometers or gradiometers, are mostly tuned to the measurement of macroscopic samples. Several groups investigate nano SQUIDs [15]-[17] for the measurement of very small magnetic moments as, e.g., single magnetic nanoparticles [17],[18] which are placed directly on the SQUID loop, partly utilizing traditional gradiometer or susceptometer concepts [19]. In this paper we present a novel high-T_c SQUID sensor concept which is based on compensating the signal in the SQUID by an inductively coupled compensation loop. Thus, this sensor possesses a high sensitivity to magnetic dipole fields but it cancels homogeneous fields and first order gradients in the symmetry direction, e.g., as produced by the magnetization coil.

All authors are with Institut für Elektrische Messtechnik und Grundlagen der Elektrotechnik, TU Braunschweig, 38106 Braunschweig, Germany (phone: +49 531 3913874; fax: +49 531 3915768; e-mail: a.guillaume@tu-bs.de).

II. Self compensating inductively coupled SQUID

A. Challenges

For the measurement of MNPs, stable operation of the sensors is required in comparably large static, ac or pulsed magnetizing fields up to the mT-range while ensuring sufficiently low 1/*f*-noise levels. An alignment of the sensor in parallel to the magnetizing field effectively reduces the noise [7], [8]. However, the alignment precision is limited by the measurement setup and thermal drift of the mechanical components. Since the relaxation signals of small amounts of particles can result in small changes of the magnetic field to be measured, the particles must be positioned close to the flux-sensitive sensor area [15]-[18]. This area must be designed with respect to the geometrical dimensions of the sample in order to achieve a suitable coupling. Additionally, disturbances – such as external magnetic fields from the environment or screening currents – must be avoided, shielded or compensated.

Planar high-T_c gradiometer designs offer the possibility to cancel out the undesired magnetic flux as long as there is no undesired spatial field gradient. However, planar gradiometers based on bicrystal high-T_c SQUIDs are generally not perfectly balanced in homogeneous fields, even for perfectly balanced pickup loops due to the non-gradiometric SQUID itself [7],[8]. Additionally, the SQUID is directly exposed to the applied magnetic field resulting in increased 1/*f*-noise.

B. SQUID Design

In order to achieve a suitable modulation depth while ensuring a reasonable white noise level and critical current densities, junctions with a width of 1.5 µm and 6 µm length are incorporated into the high-*T*c SQUID ring with an

IEEE/CSC SUPERCONDUCTIVITY NEWS FORUM (global edition) January 2015.
This ASC 2014 manuscript 2EPo1D-07 published online in IEEE Trans. Appl. Supercond.
(IEEE XPLORE) DOI: 10.1109/TASC.2014.2359764, on September 23, 2014.

inductance of around 35 pH. An average normal state resistance of 3.5 Ω is observed for our devices with an average critical current of 20 µA. The shape of the SQUID ring is a square loop design with an inner diameter of 17 µm and a linewidth of 4 µm. Thereby, variations in the diameter or linewidth have minimum effect on the SQUID area. Additionally, a less than perfect alignment of the magnetization direction of a sample relative to the SQUID has little influence on the flux coupled into the loop. A modulation depth up to 45 µV is found for a critical current of 30 µA. A superconducting stripline with linewidth 4 µm is prepared at a distance of 2 µm around the upper half of the SQUID allowing operation of the sensor in a flux locked loop (FLL) by our single channel *SEL-1* electronics from *Magnicon*. The flux coupled into the SQUID per current is given by 320 µA / Φ_0 leading to a maximum of ± 14 Φ_0 with our electronics. An external field of 4.98 µT is required to generate 1 Φ_0, thus the maximum operation range of a bare SQUID is ± 69.8 µT. The FLL is operated with a 3.3 kΩ feedback resistance in bias reversal mode at 102.4 kHz in order to reduce 1/f noise. Therefore, an operating bandwidth of typically 100 kHz can be achieved [20]. Furthermore, the effect of the magnetic field resulting from bias current and bias flux on the magnetization of the MNPs close to or on the SQUID is reduced by the bias reversal technique since the characteristic rotation frequency of the particles to be investigated at $T = 77$ K is typically in the regime of a few Hz or even lower [12].

C. Self compensation

Frequently, pickup loops are designed to maximize the effective SQUID area. The effective area for a homogenous field can be calculated as

$$A = A_S \pm L_c \frac{A_p}{L_p}, \tag{1}$$

where A_s is the SQUID area, A_p the pickup loop area, L_p the pickup loop inductance and the coupling inductance L_c. The sign of the second term is given by the position of the SQUID relative to the pickup loop. If the junctions of the SQUID are placed outside the pickup loop the "+" is used, otherwise the "−". In many cases, the SQUID area is small compared to the second term and can be neglected. By adjusting the pickup loop parameters A_p / L_p and the coupling inductance L_c, the effective area can be tuned to be near zero equivalent to a SQUID which is insensitive to an external (spatial homogenous) flux. The loop then acts as compensation loop rather than as pickup loop. However, small enough dipoles which are placed inside the compensation loop produce an overall flux of almost zero in the loop not causing any screening current or compensation. Thus, the design is sensitive to (geometrically) small magnetic dipoles placed inside the loop close to or on the SQUID.

D. Compensation loop simulation

The numeric calculations are based on the assumptions that the screening current I circulates homogeneously distributed in a thickness of $\lambda_L = 150$ nm for YBCO at the inner edges of the loop and that the resulting magnetic field B at distance r from the inner edge of the loop is given by

$$B(r) = \mu_0 \frac{I}{2\pi r} = \mu_0 \frac{B_{appl}}{2\pi r} \frac{A_p}{L_p}, \tag{2}$$

where μ_0 is the vacuum permeability $4\pi \cdot 10^{-7}$ Vs/Am and B_{appl} the applied magnetic field. A_p / L_p, the ratio of pickup loop area and inductance which determines the current in the compensation loop, is extracted from fitting the model to measured data of the compensation factor in section III. B.

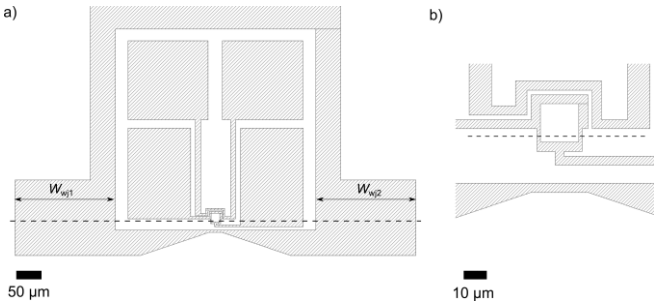

Fig. 1. a) Layout of SQUID and feedback line with bond pads inside the compensation loop, b) enlarged view of SQUID loop. Grain boundary and wide junctions ($w_{wj1} = w_{wj2}$) are drawn in.

E. Compensation loop layout

Our design under investigation employs a quadratic compensation coil with an outer diameter of 500 µm and a linewidth of 50 µm. Two different widths of the wide junctions ($w_{wj1} = w_{wj2}$) formed across the grain boundary of 50 µm and 200 µm are investigated in order to analyze their influence on the compensation. A 4 µm wide constriction is used to couple the compensation flux inductively into the sensor which is positioned inside the loop. The narrow linewidth reduces flux vortices occurring in the coupling region [21] and minimizes flux focusing effects. The coupling inductance can be tuned by varying the distance between SQUID and compensation loop. The contact pads, which are covered by silver and gold for bonding, are also located inside the compensation loop as well as the feedback line. Fig. 1 shows the layout with 200 µm wide junctions ($w_{wj1} = w_{wj2}$).

The overall flux across the SQUID is zero for optimum compensation; simulations indicate that the maximum values of the magnetic flux density are reduced to ± 0.4 B_{appl} at the edges of the SQUID. Since the SQUID is positioned in the axis of symmetry in one direction of the compensation loop, spatial first order gradient fields along this direction do not change the ratio of flux coupled into the compensation coil and into the SQUID. Thus, compensation is still active. However, spatial gradient fields along the other axis may change the ratio leading to a disturbance of the compensation.

F. Fabrication

For the fabrication of the SQUIDs, $SrTiO_3$ symmetric 10x10 mm² bicrystals (24° and 30°, respectively) are coated with a 160 nm thick YBCO thin film by pulsed laser deposition [22],[23]. In order to achieve a low contact

IEEE/CSC SUPERCONDUCTIVITY NEWS FORUM (global edition) January 2015.
This ASC 2014 manuscript 2EPo1D-07 published online in IEEE Trans. Appl. Supercond.
(IEEE XPLORE) DOI: 10.1109/TASC.2014.2359764, on September 23, 2014.

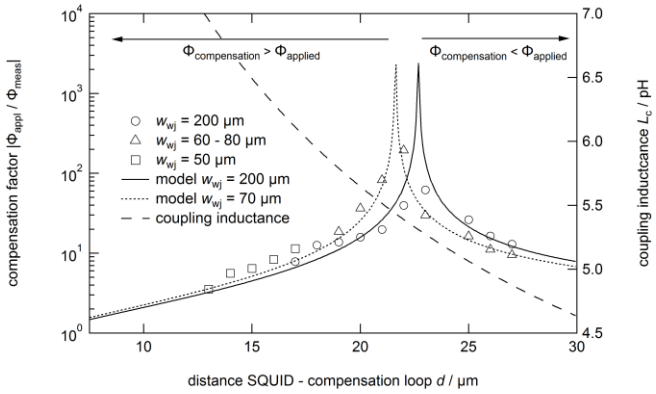

Fig. 2. Measurements, model of compensation factor and coupling inductance as function of the distance between compensation loop and SQUID for 50 µm and 200 µm wide junctions before and after etching.

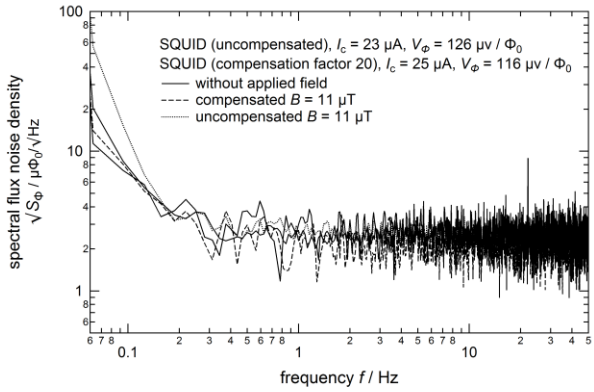

Fig. 3. Spectral flux noise density for a bare SQUID and a compensated SQUID with compensation factor 20 in zero field and in B = 11µT.

resistance and high mechanical stability of the contact pads, silver and gold is sputtered on top of the YBCO layer before patterning immediately after the YBCO deposition. Optical lithography is used in conjunction with argon ion etching to define the sensor structures. Five sensors on a chip can be characterized successively with our single channel electronics.

III. Measurements

A. Measurement setup

The setup is operated in a magnetically shielded room. Helmholtz coils with a field constant of 0.56 mT/A are used to apply a homogeneous magnetic field. The sensor is mounted on the evacuated SQUID holder perpendicular or in parallel to the magnetic field. Alignment screws allow a fine adjustment of the sensor relative to the magnetizing field, so that the field measured by the sensor in parallel orientation is reduced by a factor of more than 10^3 [12].

B. Self compensation performance

In order to determine the influence of the coupling between SQUID and compensation loop on the compensation factor, the sensors are operated in a FLL. A triangular shaped magnetic flux density ramp with a frequency of 2 Hz is applied and the response is measured. The ratio of applied flux density and the measured SQUID signal gives the compensation factor. Measurements for the layouts with 200 µm and the 50 µm wide junctions ($w_{wj1} = w_{wj2}$) were performed. Additionally, measurements on the SQUIDs with 200 µm wide junctions were carried out after reducing the width to approximately 60 to 80 µm by subsequent argon ion etching. The figure also contains calculations for the compensation factor and the coupling inductance. The ratio A_p / L_p is obtained as fit parameter, for the 200 µm wide junctions it yields 77.8 m²/H, for the narrower compensation loop junctions it amounts to 76.5 m²/H.

For the investigated coupling range, a maximum compensation factor of 195 at a distance of 22 µm is found for the design with the etched wide junctions ($w_{wj1} = w_{wj2}$) in the compensation loop. A sign change in the FLL output is observed when the coupling changes from $\Phi_{comp} > \Phi_{appl}$ to $\Phi_{comp} < \Phi_{appl}$ and vice versa, both in the simulations and in the measurements, which proofs the basic concept. Since the etched junctions exhibit a reduced ratio A_p / L_p due to the smaller flux focusing area, the optimum coupling distance is shorter than for the layout with the higher screening current. The model is in qualitative agreement with the measured data; however, there are differences. Close to the optimum compensation distance, the estimated compensation factor is overestimated for the 200 µm wide junctions while the factor is underestimated for the narrower loop. When the distance is increased or decreased for both layouts, the compensation factor is slightly underestimated. Possible reasons are the absence of flux focusing and self screening effects in the model calculations as well as the approach of the homogeneous current distribution which may affect the simulation results.

C. Noise performance

Noise measurements in FLL mode were carried out for a bare SQUID and for a SQUID with the compensation at a distance of 21 µm and having 200 µm wide junctions in the compensation loop, leading to a compensation factor of 20. In order to minimize rf-disturbances, the whole setup was wrapped in aluminum foil with a thickness of 13 µm. The low frequency spectra of both devices without applied field and in an external field magnetic flux density of 11 µT perpendicular to the sensor surface are shown in fig. 3. Both devices show a 1/f-corner frequency of below 1 Hz. The white noise level for the compensated design is approximately 2.0 $\mu\Phi_0 / \sqrt{\text{Hz}}$ while the uncompensated design shows 2.1 $\mu\Phi_0 / \sqrt{\text{Hz}}$. The critical currents of both devices are with 23 µA for the bare SQUID and 25 µA for the compensated sensor very similar, the sensitivities are estimated from $V_\Phi \approx \pi \cdot \Delta V / \Phi_0$ as 126 µV / Φ_0 and 116 µV / Φ_0, where ΔV is the peak-to-peak modulation of the flux-voltage curve [24]. For the devices, no increase in the 1/f-noise down to 0.15 Hz is observed when a magnetic flux density of 11 µT is applied.

D. Design limitation

When the magnetic field is increased above a critical magnetic flux density, which is determined by the relation of the current circulating in the compensation loop and the

IEEE/CSC SUPERCONDUCTIVITY NEWS FORUM (global edition) January 2015.
This ASC 2014 manuscript 2EPo1D-07 published online in IEEE Trans. Appl. Supercond.
(IEEE XPLORE) DOI: 10.1109/TASC.2014.2359764, on September 23, 2014.

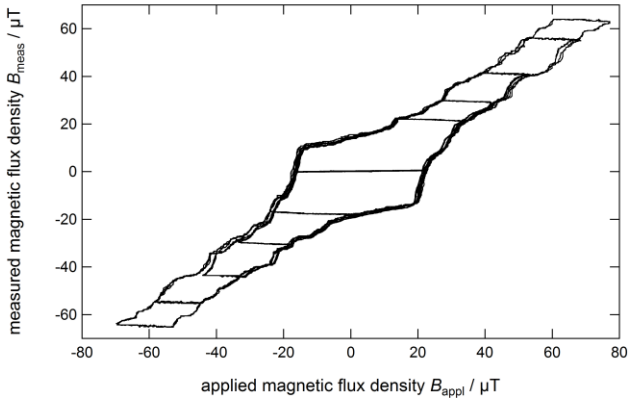

Fig. 4. Measured magnetic flux density over applied magnetic flux density for the compensated design with 200 µm wide junctions and a compensation factor of 28. A hysteresis arises when the peak value of the magnetic field is increased above the breakdown field, e.g. ± 13 µT for the presented measurement.

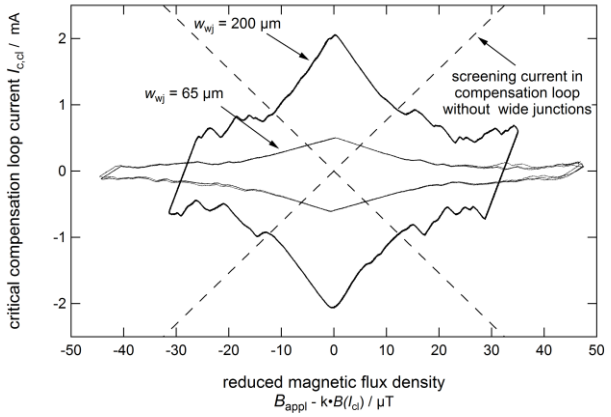

Fig. 5. Screening current in the compensation loop and Fraunhofer pattern for the wide junctions before (w_{wj} = 200µm) and after etching (w_{wj} = 65µm), calculated by equation (3).

magnetic field dependent critical current of the wide junctions, the compensation effect of the loop vanishes. In order to investigate the compensation current behavior we operated the SQUID in FLL mode and recorded the output for various peak amplitudes of the applied triangular magnetic flux density. A hysteresis in the FLL output arises when the critical magnetic flux density is reached as shown in fig. 4.

When the screening current $I_p = B_{appl} \cdot A_p / L_p$ in the loop exceeds the critical current of one of the two wide junctions, the compensation breaks down. As the applied flux is further increased, flux quanta enter the compensation loop. For each flux quantum, the screening current is reduced by Φ_0/L_p corresponding to change of a few µA. Since the critical current is in the order of mA, these small changes cannot be observed directly in the measurements so that the difference between measured and applied magnetic flux density is essentially given by the critical current of the compensation loop. Thus, the magnetic field dependent critical current of the compensation loop can be computed from the difference between the applied flux density and the measured hysteretic behavior of the measured signal by

$$I_{c,\,cl}(B_{appl}) = \frac{B_{meas} - B_{appl}}{L_c} A_{eff,\,s}, \qquad (3)$$

where $A_{eff,s}$ = (20.4 µm)² is the effective SQUID area. In order to account for the self-screening effects introduced by the loop current, the resulting curves are plotted against the reduced magnetic flux density $B_{appl} - k \cdot B(I_{cl})$. k is an empirical factor between 0.45 and 0.48 for the 200 µm junctions and between 0.32 and 0.35 for the etched, 60 - 80 µm junctions. When the applied magnetic flux density slope changes direction at a value B, the compensation current is reduced below the critical current. As the applied magnetic flux density is increased again by approximately $2 \cdot I_{c,cl}(B) \cdot L_p / A_p$, the critical current with opposite direction is exceeded. The calculations result in a nearly symmetric triangular shaped Fraunhofer pattern which is well known for wide junctions. Fig. 5 shows the pattern for a compensation loop before and after etching of the wide junctions including the screenings current that would occur without wide junctions in the loop. The obtained values for the critical current at zero applied field are in agreement with the values from literature for wide junctions with comparable width at T = 77 K [25]. When the magnetic flux density is increased from zero, the magnetic field required for compensation breakdown is given by the intersections of the loop screening currents and the critical current of the compensation loop. The critical current is reduced according the reduction of the junction width after etching by a factor of approximately 2.6 to 3.1. In the region around zero magnetic field, the slope of the curves is nearly linear and scales with the width of the junctions, resulting in a steeper slope for the 200 µm junctions. Fraunhofer patterns were recorded for several junctions before and after etching. The critical currents at zero field are in a range from 0.43 mA to 2.11 mA, the corresponding critical currents for the compensation breakdown are reduced according to the reduction of $I_{c,cl}(0)$ after etching. For most sensors, the magnetic flux density required for compensation breakdown is approximately 10 µT or larger before etching and 5 µT or larger after etching.

IV. Summary and Conclusion

The measurements of the compensation factor are in agreement with the models and proof the basic design concept. A maximum of compensation factor of 195 was observed. No increase in the low frequency noise was recorded when the SQUID was operated in a perpendicular field of 11 µT. The compensation vanishes in applied magnetic flux densities of at least 5 µT and 10 µT, respectively, caused by the screening current of the loop exceeding the field dependent critical current of the wide junctions. It can be concluded, that the SQUID with compensation is suitable for the operation in mT-field when a parallel alignment of the field relative to the SQUID surface by an addional factor of 10^2 to 10^3 is possible which can be achieved with a relatively simple mechanical setup [12].

Acknowledgment

The authors want to thank Dr. Thomas Weimann from the PTB Braunschweig for the fabrication of the optical lithography masks and Dr. Henry J. Barthelmess for help with modification of the FLL electronics.

IEEE/CSC SUPERCONDUCTIVITY NEWS FORUM (global edition) January 2015.
This ASC 2014 manuscript 2EPo1D-07 published online in IEEE Trans. Appl. Supercond.
(IEEE XPLORE) DOI: 10.1109/TASC.2014.2359764, on September 23, 2014.

REFERENCES

[1] F. Ludwig, E. Heim, and M. Schilling, "Characterization of superparamagnetic nanoparticles by analyzing the magnetization and relaxation dynamics using fluxgate magnetometers", *J. Appl. Phys.*, vol. **101**, pp. 113909-1–10, 2007.

[2] R. Kötitz, T. Bunte, W. Weitschies, and L. Trahms, "Superconducting quantum interference device-based magnetic nanoparticle relaxation measurement as a novel tool for the binding specific detection of biological binding reactions*", J. Appl. Phys*., vol. **81**, p. 4317, 1997.

[3] H. Matz, D. Drung, S. Hartwig, H. Groß, R. Kötitz, W. Müller, A. Vass, W. Weitschies, and L. Trahms, "A SQUID Measurement System for Immunoassays", *Appl. Supercond.*, vol. **6**, pp. 577-583, 1998.

[4] D. Eberbeck, F. Wiekhorst, U. Steinhoff, and L. Trahms, "Aggregation behaviour of magnetic nanoparticle suspensions investigated by magnetorelaxometry", *J. Phys.: Condens. Matter* **18**, pp. 2829-2846, 2006.

[5] M. Büttner, F. Schmidl, M. Schiffler, and P. Seidel, "Magnetorelaxation (MRX) Measurements with DC-SQUID Gradiometers", *IEEE Trans. Appl. Supercond*., vol. **21**, pp. 473-476, 2011.

[6] A. Haller, S. Hartwig, H. Matz, J. Lange, T. Rheinländer, R. Kötitz, W. Weitschies and L. Trahms, "Magnetic nanoparticle relaxation measured by a low-T_c SQUID system", *Supercond. Sci. Technol.* **12**, pp. 956-958, 19999.

[7] Y. R. Chemla, H. L. Grossman, Y. Poon, R. McDermott, R. Stevensi, M. D. Alper, and J. Clarke, "Ultrasensitive magnetic biosensor for homogeneous immunoassay", *PNAS*, vol. **97**, pp. 14268-14272, 2000.

[8] H. L. Grossman, W. R. Myers, V. J. Vreeland, R. Bruehl, M. D. Alper, C. R. Bertozzi, and John Clarke, "Detection of bacteria in suspension by using a superconducting quantum interference device", *PNAS*, vol. **101**, pp. 129-130, 2004.

[9] K. Enpuku, T. Minotani, M. Hotta, and A. Nakahodo, "Application of High Tc SQUID Magnetometer to Biological Immunoassays*", IEEE Trans. Appl. Supercond.*, vol. **11**, pp. 661-664, 2011.

[10] K. Enpuku, D. Kuroda, T. Q. Yang, and K. Yoshinaga, "High T_c SQUID System and Magnetic Marker for Biological Immunoassays", *IEEE Trans. Appl. Supercond*., vol. **13**, pp. 371-376, 2003.

[11] K. Enpuku, and T. Minotani, "Biological Immunoassay with High T_c Superconducting Quantum Interference Device (SQUID) Magnetometer*", IEICE Trans. Electron.*, vol. **E84-C**, pp. 43-48, 2001.

[12] A. Guillaume, F. Ludwig, J. M. Scholtyssek and M. Schilling,"Field stability of a directly coupled high-T_c SQUID design regarding MRX measurements", *IEEE Tran. Appl. Supercond.* **23**, No.3, 2013.

[13] S. Lee, W.R. Myers, H. L. Grossmann, H.-M. Cho, Y. R. Chemla and J. Clarke, "Magnetic gradiometer based on a superconducting high-transition temperature superconducting quantum interference device for improved sensitivity of a biosensor", *Appl. Phys. Lett* . **81** (16), pp. 3094-3096, 2002

[14] E. Dantsker, O. M. Froehlich, S. Tanaka, K. Kouznetsov, J. Clarke, Z. Lu, V. Matijasevic and K. Char, "High-Tc superconducting gradiometer with a long baseline asymmetric flux transformer", *Appl. Phys. Lett.* **71** (12), pp. 1712-1714, 1997.

[15] T. Schwarz, J. Nagel, R. Wölbing, M. Kemmler, R. Kleiner and D. Koelle, "Low-noise nano superconducting Quantum Interference Device operating in Tesla magnetic fields", *ACS Nano* **7**, No. 1, pp. 844-850, 2013.

[16] A. G. P. Troeman, H. Derking, B. Borger, J. Pleikies, D. Veldhuis and H. Hilgenkamp, "NanoSQUIDs based on Niobium constrictions", *Nano Lett.***7**, No. 7, pp. 2152-2156, 2007.

[17] L. Hao, D. Cox, P. See, J. Gallop and O. Kazakova, "Magnetic nanoparticle detection using nano-SQUID sensors", *J. Appl. Phys.* **43**, 2010.

[18] W. Wernsdorfer, K. Hasselbach, D. Mailly, B. Barbara, A. Benoit, L. Thomas, and G. Suran, "DC-SQUID magnetization measurements of single magnetic particles", *J. Magn. Magn. Mater.* vol. **145**, pp. 33–39, 1995.

[19] D. Drung, J.-H. Storm, F. Ruede, A. Kirste, M. Regin, T. Schurig, A. M. Repollés, J. Sesé, and F. Luis, "Thin-film microsusceptometer with integrated nanoloop", *IEEE Tran. App. Supercond.* **24**, No. 4, August 2014.

[20] D. Drung, "High-T_c and low- T_c dc SQUID electronics", *Supercond. Sci. Technol.* **16**, pp. 1320-1336, 2003.

[21] E. Dankster, S. Tanaka, P.-A. Nilsson, R. Kleiner and J. Clarke, "Reduction of 1/f noise in high T_c dc superconducting quantum interference devices cooled in ambient magnetic field", *Appl. Phys. Lett.* **69**, pp. 4099-4101, 1996.

[22] J.-K.Heinsohn, D. Reimer, A. Richter, K. O. Subke and M. Schilling, "Interaction of process parameters in the pulsed laser deposition of $YBa_2Cu_3O_x$ films", *Physica C* **299**, pp. 99–112, 1998.

[23] M. Schilling, A. Guillaume, J. M. Scholtyssek and F. Ludwig, "Design of experiments for highly reproducible pulsed laser deposition of $YBa_2Cu_3O_{7-\delta}$", *J. Appl. Phys.* **47**, 2014.

[24] D. Koelle, R. Kleiner, F. Ludwig, E. Dantsker and J. Clarke, "High-transition-temperature superconducting quantum interference devices", *Rev. Mod. Phys* **71**, no. 3, pp. 631-678, 1999.

[25] B. Mayer, S. Schuster, A. Beck, L. Alff and R. Gross, "Magnetic field dependence of the critical current in $YBa_2Cu_3O_{7-\delta}$ bicrystal grain boundary junctions", *Appl. Phys. Lett* **62** *(7)*, pp. 783-785, 1993.